Corrosion Resistance of Reinforcing Steel in Concrete Using Natural Fibers Treated with Used Engine Oil

Alejandro Flores Nicolás [1*], Elsa. C. Menchaca Campos [1], Mario Flores Nicolás [2],
Omar A. Gonzalez Noriega [1], Cesar A. García Peréz [1], Jorge Uruchurtu Chavarín [1]

[1] *Centro de Investigación en Ingeniería y Ciencias Aplicadas, Universidad Autónoma del Estado de Morelos, Cuernavaca, 62209, México.*

[2] *Instituto de Ingeniería, Universidad Nacional Autónoma de México, Cdmx, 04510, México.*

Abstract

The addition of natural fibers in the elaboration of concrete pastes has increased as an innovative alternative for the development of more ecological and environmentally friendly constructions. The objective of this research is to incorporate natural fiber residues from palm leaves and mango stone impregnated with used engine oil (UEO) in the cement matrix to improve the mechanical and electrochemical properties of reinforced concrete. Samples with fiber percentages of 0.2% and 0.4% with respect to the weight of the sand with a length of 10 mm were fabricated. Their properties, such as workability, air content, porosity, and compressive and flexural strength, were analyzed. To understand the corrosion rate of the steel bars, electrochemical techniques of corrosion potential, electrochemical noise, linear polarization resistance, and electrochemical impedance spectroscopy were applied to cubic samples exposed in a 3% sodium chloride saline environment for 365 days. The experimental results showed a positive effect on the corrosion phenomenon with the UEO and mango fiber treatment, decreasing the corrosion rate due to the formation of a protective film at the steel/concrete interface.

Keywords: Concrete; Natural Fibers; Corrosion; Used Engine Oil; Surface Treatment; Electrochemical.

1. Introduction

Concrete is a material used in construction due to its excellent mechanical properties in compression, and combined with reinforcing steel, the material acquires high tensile strengths. The cement paste passivates the steel, protecting it from corrosion agents due to its high alkalinity, which promotes a protective oxide layer that separates it from highly aggressive environments. However, corrosion of steel reinforcement and other embedded metals is the main cause of poor performance and durability problems in reinforced concrete (RC) structures [1]. The passive layer protecting the rebar is easily destroyed by carbonation and/or the presence of chlorides. Corrosion products occupy a larger volume than the original; internal steel corrosion products promoting tensile stresses will accumulate in the concrete [2]. After the passive layer is destroyed, a visible sign of corrosion appears on the surface of the structure, e.g., cracks, rust stains, concrete spalling, etc. [3]. To reduce the effects of corrosion, the need to obtain synthetic, natural, or waste materials as alternatives to conventional reinforced concrete has been sought [4].

The advantage of using natural waste as an alternative is its positive impact on the environment, which can be obtained at a low cost using traditional knowledge and practices [5–7]. How these natural materials are included in the concrete is through fibers such as jute [8], bamboo [9], coconut [10], palm [11], sugarcane bagasse [12], and others,

which have several advantages, including low density, high flexural strength, flexibility, and high elastic modulus [13]. These fibers consist of cellulose micro-fibrils suspended in a matrix of amorphous lignin/hemicellulose composition, which gives the natural fibers their chemical composition [14]. The introduction of new types of vegetable fibers to concrete has been investigated as it has a great perspective and potential in the construction sector. Vegetable fibers from palm leaves and mango stones are innovative agricultural residues that can be used in adequate quantities as concrete reinforcement, although they present durability problems. Water absorption is one of the main problems of natural fiber composites, which reduces their mechanical properties and dimensional stability, limiting their use in various applications [15–17].

Zhan et al. [18] explored the effect of natural jute fibers on compressive strength, and the results are critical because natural fibers swell by absorbing water (during casting and their lifetime), creating spaces between the fibers and the matrix. Shah et al. [19] observed that increasing the concentration of natural fiber decreased the settlement values in all specimens. These reported decreases in workability are the result of moisture absorption by hydrophilic natural fibers [20]. Numerous researchers have incorporated chemical or physical treatments into natural fibers to protect them from water absorption and avoid disadvantages such as fiber/cement biocompatibility [21, 22]. Used engine oil (UEO), generated by industrial activity and transportation around the world, generates great pollution because it is discharged specifically into groundwater and soil, generating high levels of carbon dioxide [23, 24]. This material can be added as a natural fiber treatment because it is a hydrophobic material, does not require a manufacturing process, and is an attractive option for the elimination of OEU. Juarez Alvarado et al. [6] used hydrophobic substances: linseed oil, linseed oil + natural resin, kerosene, kerosene + natural resin, wood sealant, and creosote as surface treatments for the lechuguilla fibers to reduce the absorption of water, concluding that the protective treatment with kerosene reduced the absorption capacity of the natural fiber.

Yousif et al. [25] studied the treatment of kenaf fibers immersed in 4 solutions: water, salt water, diesel, and engine oil, and obtained the conclusion that oil and diesel had a lower absorption rate of 20−30% compared to the untreated fiber of 90%, although it reduced the tensile strength. Wong et al. [26] evaluated the effects of fiber treatment on absorption in motor oils and petroleum, and their results showed that vegetable fibers have increased oil absorption, which reduces water absorption. Ramli et. al. [27] evaluated coconut fibers incorporated in concrete with a percentage of silica fume as a binder and reported that, for more severe climates such as seawater chlorides, two factors influence the chloride penetration of concrete: the severity of exposure to the chloride source and the permeability of the specimens. However, the impact of the use of natural fibers treated with UEO on the corrosion of cementitious elements is still not clearly known.

The mechanical properties of concrete with natural fibers are variable; however, the scenarios and aggressive environments are still not clearly known. This work will take an innovative approach and provide further insight into the current literature on steel corrosion phenomena, so this research study describes the use of two natural fibers (mango stone and palm leaf) treated superficially with used engine oil (UEO) and used as reinforcements in concrete to improve mechanical and electrochemical properties such as compressive strength, flexural strength, and corrosion rate resistance.

2. Materials and Methods

2.1. Materials

Portland cement CPC 30 R was used for concrete sample preparation; according to the international ASTM C150 standard [28], river sand was used as fine aggregate with a 4.75 mm maximum particle size, crushed gravel (19 mm nominal size) as coarse aggregate, tap water, and natural fibers. The general methodology of the work is shown in the flowchart in Figure 1.

2.2. Fibers

Two types of fibers were used in the concrete: mango fibers (CMF) and palm fibers (CPF). Mango stone residues are considered as wastes, and solitary hermaphrodite Mexican Sabal palm are considered important component sources [29], distributed across the USA, Mexico, and Central America down to Venezuela and Colombia [30]. Both materials were cleaned, eliminating polluting residues, and afterward were dehydrated at room temperature for three days. The hollow tubular structure of the fibers also reduces their volume and density and makes them lighter [31], having different values as shown in Table 1.

Table 1. Fiber density

Fiber	Density (g/cm^3)	Fiber Type	Reference
Mango	0.91-1.08	Woody	[32]
Palm leaf	0.5-0.8	Leaf	[11]

Short fibers were cut manually with dimensions of 10 mm in length and 3-4 mm in width, and 0.1 mm in thickness and presented in Figure 2.
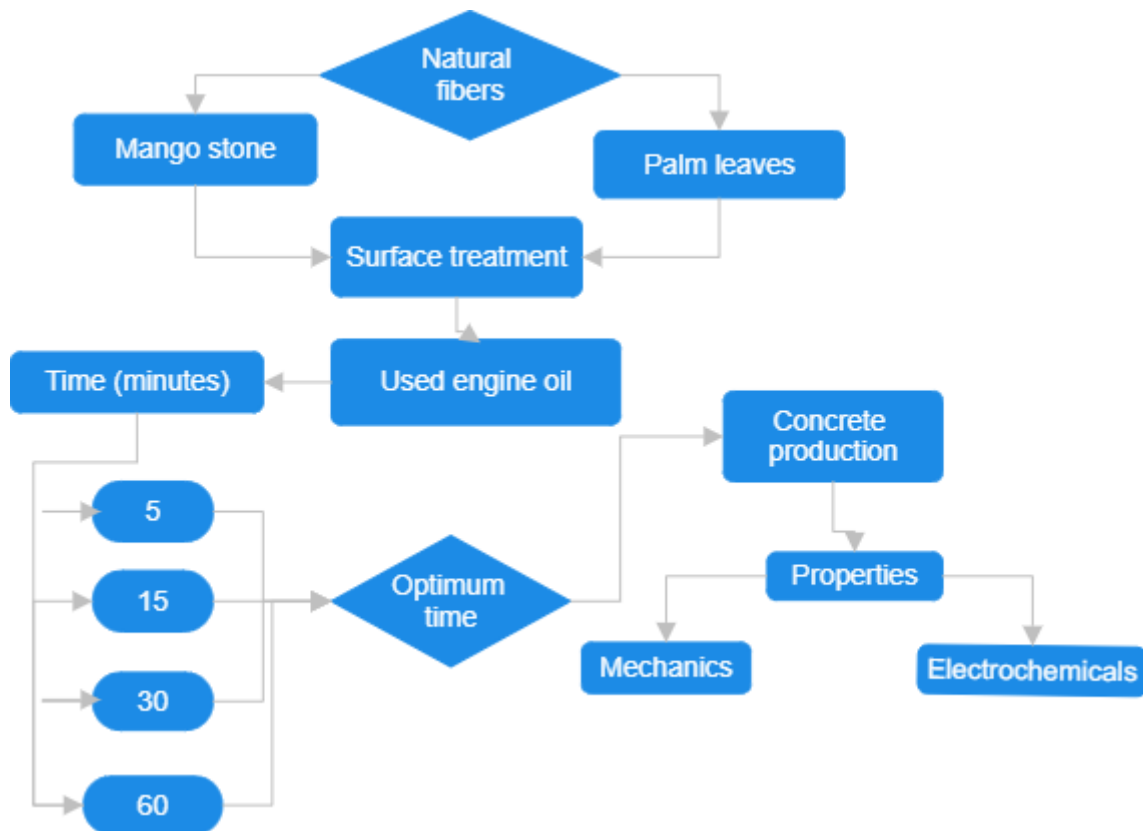
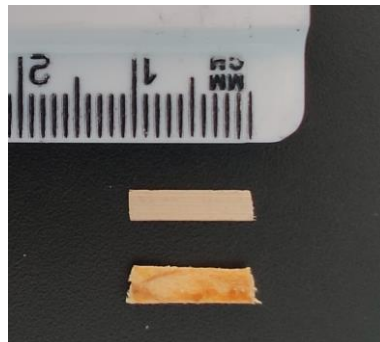**Figure 1. Flowchart of the experimental methodology**

Figure 2. Measurements of natural fibers

2.3. Fibers Treatment

Fiber chemical treatment alters superficial energy and structural characteristics through the shallow cellular walls surfaces modification, without deteriorating its chemical composition [33]. The hydrophobic characteristic substance was used, being easy to obtain, recycled, and economical, with the purpose of reducing high water absorption, giving protection at high alkaline concrete. The UEO chemical properties are shown in Table 2.

Table 2. Used motor oil chemical properties

Chemical composition	Used engine oil (%)	Reference
Sulfur (SO_3)	31- 37	[34, 35]
Chloride (Cl-)	14.9-15.9	[34, 35]
Lead content (mg/kg)	3.6	[34]
Zinc (ZnO)	17.7-19.2	[34, 35]
Nitrite (Ni)	5.5	[34]
P_2O_5	8.95	[35]
Others	4.12	[35]

Natural fibers surface treatment (TNF) using capillary impregnation using 30 CMF fiber or 50 CPF fiber strips. Afterwards, they were immersed in UEO at 70 °C temperature for 5, 15, 30, and 60 minutes as shown in Figure 3. These times are considered to obtain the best conditions to penetrate fibers completely and less natural fibers water absorption.
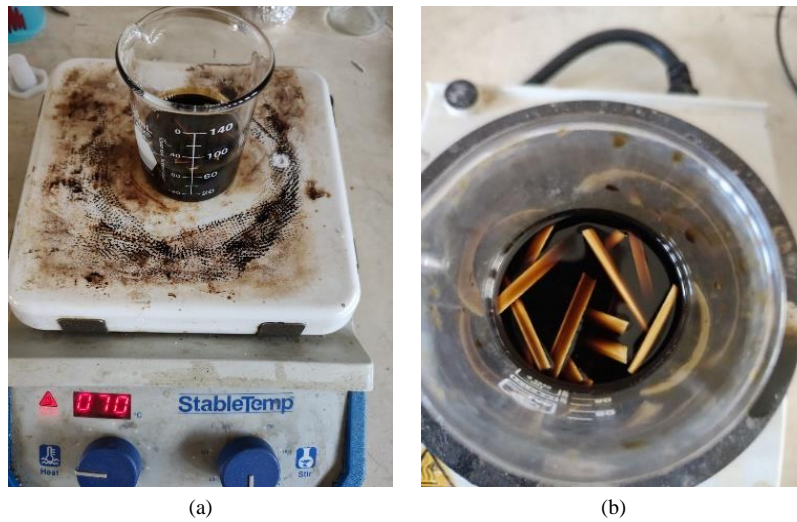

(a)   (b)

Figure 3. a) Surface impregnation of the fibers b) Fiber saturation

Afterward, humidity absorption was determined, by saturating fibers in distilled water for 24 hours, removing them, and cleansed with an absorbent cloth to retire UEO excess until obtaining dry superficial fibers, as seen in Figure 4. Then fibers were weighed on a 0.0001 g precision Denver Instrument electronic scale. The samples were dried again at 70 °C for one hour and weighed again.

Figure 4. Surface drying of treated fibers

For the calculation of water absorption percent (Wa %) Equation 1 was used, where W is the saturated water humidity weight and Wo dried weight at 70 °C [36-38]:

$$\text{Wa}\% = \frac{W - W_0}{W_0} \times 100 \tag{1}$$

Table 3 presents the natural fiber superficial treatment average absorption percent in 5, 15, 30, and 60 minutes immersed in UEO. In general, it can be appreciated the different percentages of mango and palm natural fibers, noticing fibers without treatment absorb a greater water quantity due to the presence of waxes and threads in the external layer from untreated fibers absorbing more from the solutions [25]. The water absorption diminished in treated fibers at 15 minutes immersed in the hydrophobic medium; that is, the treatment time presents a better response to the absorption resistance material as compared with untreated fiber absorption, therefore this immersion time was selected for concrete preparation.

Table 3. Absorption average percent for natural fibers

		Absorption in %			
		Treatment (minutes)			
Fiber	**Untreated**	**5**	**15**	**30**	**60**
CMF	39.24	34.69	31.24	29.84	29.92
CPF	56.91	37.71	37.64	45.64	50.33

2.4. Concrete Preparation

Table 4 presents the dosage for 80 liters of concrete using the absolute volumes method. A 300 kg/cm^2 (29.44 MPa) theoretical mix adding up fiber percents of 0.2 or 0.4 with respect to the sand weight, with 0.54 water/cement relation, without any additive.

Table 4. Concrete proportions for 80 liters

Material	C	0.2% fiber	0.4% fiber
Cement (Kg)	29.286	29.286	29.286
Water (l)	15.811	15.811	15.811
a/c	0.54	0.54	0.54
Sand (Kg)	52.049	51.947	51.842
Gravel (Kg)	83.811	83.811	83.811
Fiber (Kg)	0	0.104	0.208

Five mix designs were prepared, two mixtures of concrete with mango fibers (CMF,) in two percentages mentioned, and two mixtures of palm fiber (CPF) and control concrete (C). The nomenclature of the samples is specified in Table 5.

Table 5. Identification for samples

Material	Type of fiber	Percentage (%)	Nomenclature
	--	--	C
Cement	Mango	0.2	CMF-02
		0.4	CMF-04
	Palm	0.2	CPF-02
		0.4	CPF-04

The mixture was prepared as follows: first gravel, after a small quantity of water was poured. Then sand was added, then the cement, and finally the rest of the water incorporating the TNF. Physical tests such as air contained in the mixture, according to the standards [39, 40], as seen in Figure 5. Cylindrical specimens were prepared with standard dimensions of 15 cm diameter and 30 cm height [41] for 7 and 28 days of compression testing.
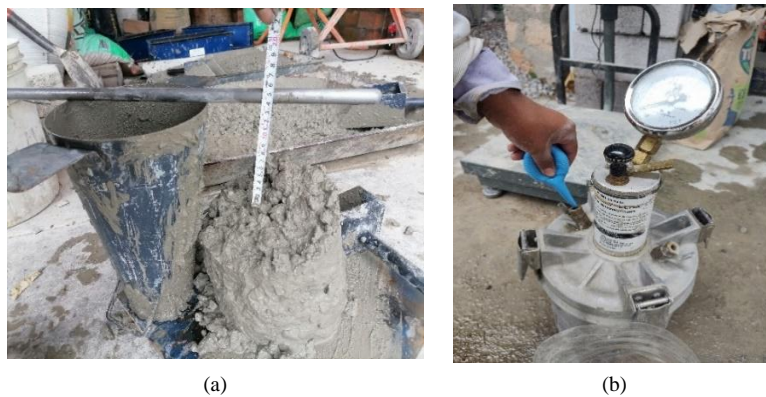

(a)   (b)

Figure 5. a) Slump test b) Air content

Samples were transported and kept in adequate conditions of humidity, and curing for 28 days. For flexural tests, concrete blocks 50 cm long, 15 cm wide, and 15 cm high were manufactured [41] for 28 days resistance test. A universal press with 120 tons maximum capacity was used for mechanical concrete tests. The standard procedure was used [42, 43] (load at third points) and flexural resistance was calculated using Equation 2:

$$f'f = \frac{PL}{bd^2} \tag{2}$$

where $f'f$ is the flexural resistance, P is the applied load, L is the distance between supporting points, b is the width, and d is the average slope of the sample as shown in Figure 6.

Figure 6. Concrete flexural strength test

Cubic samples were made for the electrochemical tests, with dimensions of 12 cm length, 8 cm width, and 12 cm height as shown in Figure 7, and three low carbon steel rods were embedded. The steel rods were named working electrodes W_1 and W_2, and a third rod was used as an auxiliary electrode according to the electrochemical cell proposed for the different measurement techniques. The coating of the paste with the steel bar was 3.5 cm, simulating a structural element, and Teflon tape was placed at the steel/paste interface in order to avoid contamination or any alteration in the measurements. The contact area of the rebar embedded in the concrete is 22.30 cm^2. The specimens were transported to a place with adequate humidity conditions, curing for 28 days.
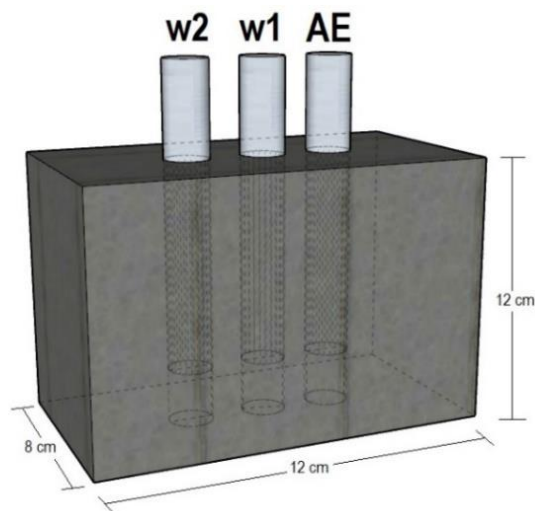

Figure 7. Sample dimension for electrochemical tests

3. Electrochemical Techniques

3.1. Hall-Cell Open Circuit Potential

The E$_{corr}$ corrosion potential, also known as half-cell potential (HCP), is the open circuit potential (OCP) of the rebar [44]. ASTM C876-09 [45] relates HCP to the probability of corrosion of reinforcing bars in concrete. With the values obtained, it is feasible to elaborate a diagnosis of the degree of corrosion risk of the concrete reinforcement [46]. The electrochemical cell for HCP monitoring was made with a saturated silver/silver chloride reference electrode (Ag/AgCl) and a working electrode W, both electrodes were connected to a multimeter. The measurement started 24 hours after the immersion of the specimens in the saline solution, the interpretation of the data is the average of the measurements of the 3 steel rods. Table 6 shows the parameters for interpreting the corrosion potential in reinforced concrete.

Table 6. Corrosion potential parameters E$_{corr}$

Reference electrode Ag/AgCl (mV)	Corrosion risk (%)
less than −150	10% Corrosion probability
−150 to −300	Uncertain zone
more than −300	90% Corrosion probability

3.2. Electrochemical Noise

The method involves the measurement of small fluctuations in the current signals created between two nominally identical electrodes, and the voltage signals that are generated between the reference electrode and the working electrodes [47]. The electrochemical cell connection for the other electrochemical techniques is described in Figure 8, two working electrodes W_1 and W_2 were used as corrosive working elements, a reference electrode (RE) Ag/AgCl was used, and closing the circuit a third rod was used as auxiliary electrode (AE). A Gill AC-ACM Instruments device was used, and measurements of 1024 readings were taken at a standard rate of 1 reading/second.
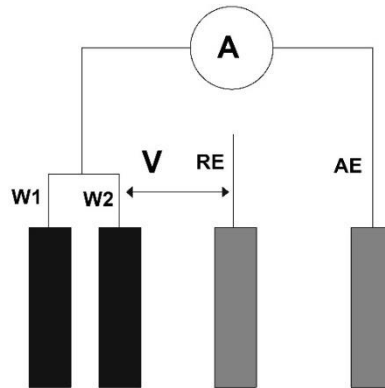

Figure 8. Electrochemical cell configuration

The electrochemical noise resistance (Rn) was calculated with the quotient of the standard deviations of potential (σv) over current (σi).

$$R_n = \frac{\sigma v}{\sigma i} \tag{3}$$

Another statistical data that can be obtained with Rn measurements is the localization index, which is related to the type of corrosion that occurs: generalized (value close to 0) or localized (value close to 1) [48]. Table 7 shows the range of values for the different types of corrosion that occur in the steel bar.

Table 7. Range of current values for the type of corrosion

Location index values	type of corrosion on the steel surface
0.001 - 0.01	Generalized
0.01 –0.1	Mixed
0.1 – 1	Localized
> 1	Start of pitting

The corrosion rate, V_{corr} represents the volumetric loss of metal per unit area and unit time, and is obtained from the corrosion current, through Faraday's law, and the density of the metal, for steel, 1 µA/cm^2 is equivalent to a corrosion rate of 0.0116 mm/year [49]:

$$V_{corr}\left(\frac{mm}{year}\right) = 0.116 * I_{corr}\left(\frac{\mu A}{cm^2}\right) \tag{3}$$

3.3. Linear Polarization Resistance

A Gill AC-ACM instruments potentiostat was used to measure the LPR technique, the layout of the electrochemical cell is described in the preceding section, a small amplitude of potential values of -50 mV and +50 mV were applied close to E$_{corr}$, by ASTM G-59 standard [50], and a sweep rate of 60 mV/min.

The polarization resistance Rp was calculated according to Equation 5, which defines the tangent of the polarization curve in the anodic and cathodic regions in the narrowest possible polarization range around the corrosion potential [51, 52]. To obtain I_{corr}, the polarization resistance (Rp) is related to Stern-Geary, then the constant B depends on the anodic and cathodic Tafel slope constants, According to Equation 6, the guidelines for measuring I_{corr} adopt the values of B as 26 and 52 mV for active and passive steels, respectively [53, 54]:

$$R_p = \frac{dE}{di} \tag{4}$$

$$I_{corr} = \frac{babc}{2.303(ba+bc)} = \frac{B}{R_p} \tag{5}$$

According to Andrade & Alonso [49], a current density ratio I_{corr} can be obtained to estimate the degree of corrosion and durability of reinforced concrete structures, parameters as shown in Table 8.

Table 8. Electrochemical parameters of I_{corr} on the service life of reinforced concrete

I_{corr} (µA/cm²)	Degree of corrosion in the metal
< 0.1	Negligible
0.1 –0.5	Moderate
0.5 – 1	High
> 1	Very High

3.4. Electrochemical Impedance Spectroscopy

Electrochemical impedance spectroscopy (EIS) is a non-destructive testing method that uses low amplitude and variable frequency sweep alternating currents to study the properties of materials [55]. It can be considered an informative method because does not only measures the polarization resistance but also evaluates the physical processes within the concrete and at the steel/concrete interface [56]. The EIS measurement technique sweep was performed in a frequency range of 0.01 Hz (low) to 10000 Hz (high), and a sinusoidal perturbation of ± 20 mV was applied, with the support of potentiostat equipment attached to a computer and appropriate software.

4. Results and Discussion

4.1. Physical Properties of Fiber-Reinforced Concrete

The slump test is used to evaluate the consistency or workability of the concrete mix. The workability is an indicator of quality control of materials such as fine and coarse aggregates with the cementitious matrix [4]. Workability concrete results are shown in Figure 9 where the concrete control presents a 14 cm slump effect, and when adding treated natural fibers (TNF) an annealing increase due to the reduction in water quantity was obtained, and a consequence of UEO acting as a water reducer during the curing process, and the increase in a slump from high contents of SO_3 in UEO [35, 57]. It was shown that the UEO particles act as a super-plasticizer in the concrete mix and these results are in agreement with other authors [58, 59]. The results for air content are shown in Figure 10, where it can be observed that the specimens with treated fibers increased the amount of voids in the cementitious matrix, which could indicate that the use of WEU caused a bad interaction between the paste and the fiber, i.e., the adhesion decreased drastically for samples CPF-02 and CPF-04 with air content values of 133% and 123% with respect to the control sample, showing that the increase of UEO absorption increases the air content.
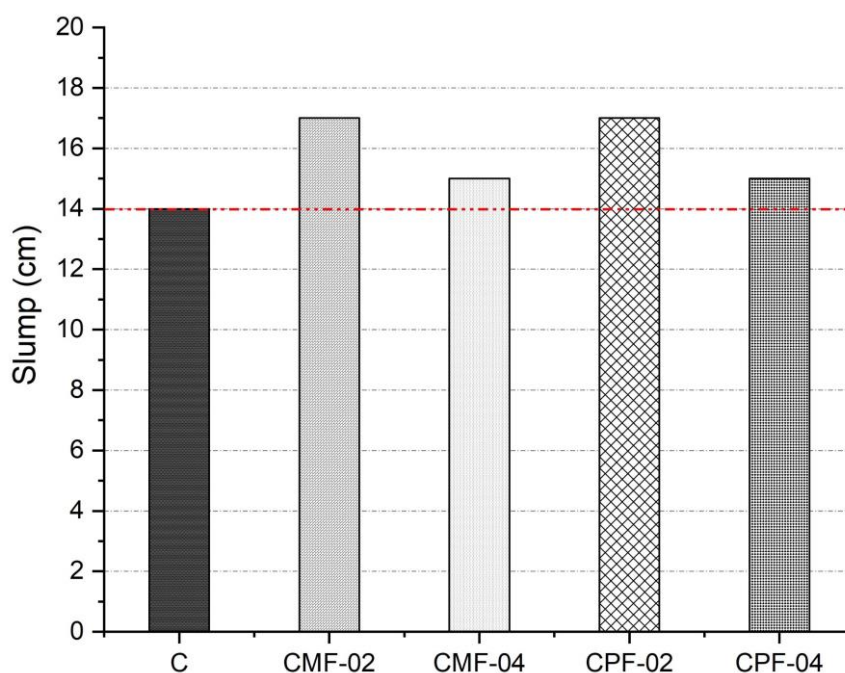

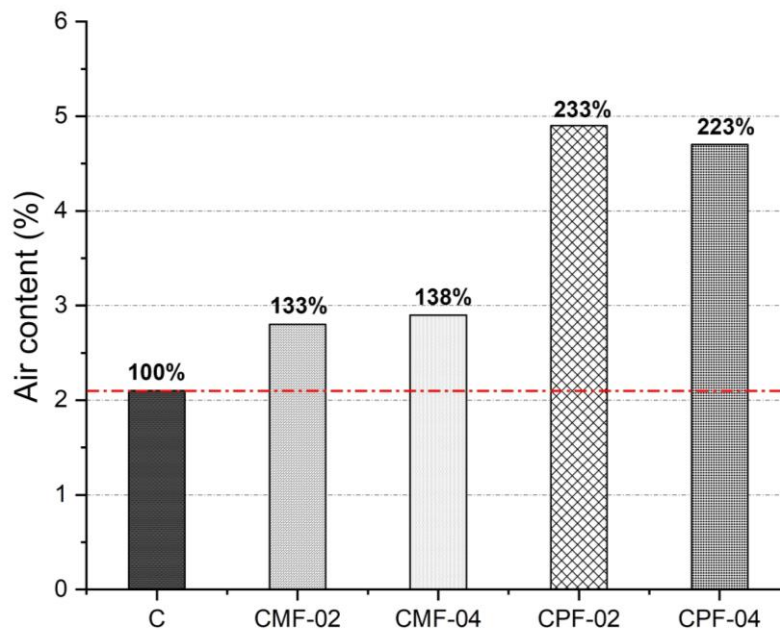**Figure 9. Slump variation in concrete with TNF**

Figure 10. Air content in concrete with UEO-treated fibers

In the complex concrete microstructure, pores may be present in nanometers up to the macro scale [60], and porosity was obtained from air content results [61]. Figure 11 presents the concrete porosity results, where sample C shows 19% porosity, with an a/c relation of 0.54, being this result similar as reported by other authors [46, 62, 63]. All samples with TNF present more void content when compared to the control sample provoking an increase in permeability, directly affecting its compression resistance [64]. It can be appreciated that CPF-02 and CPF-04 samples present a higher percent porosity of 34% and 32%, possibly due to UEO directly affecting the interfacial zone between the aggregates and fibers matrices.
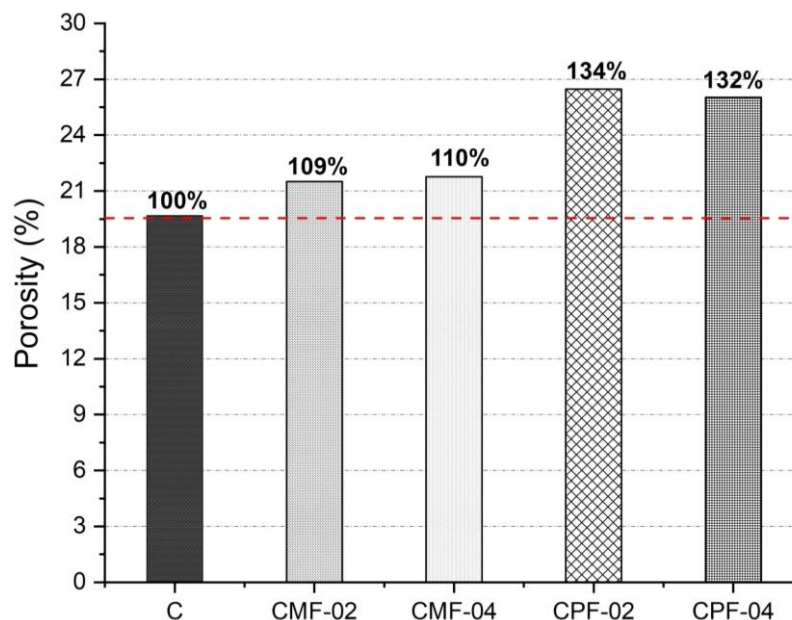

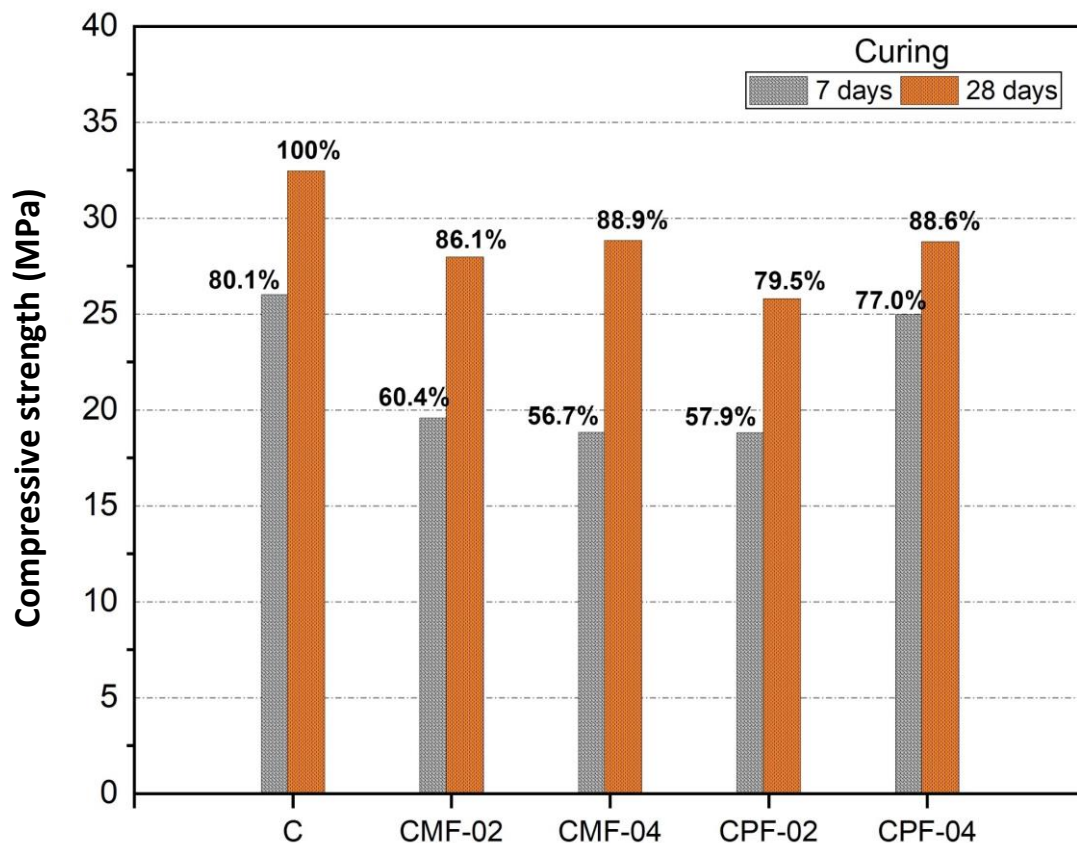**Figure 11. Percentage porosity of concrete with TNF**

4.2. Compressive Behavior of Concrete Specimens

Average compression resistance results obtained at 7 and 28 curing days are presented in Table 9. The control sample presents a higher compression resistance (F´c) as compared to the other samples, due to the presence of UEO from natural fibers; this is due to the increase in the interfacial transition zone (ITZ) surrounding the aggregates with the fiber. A greater ITZ presents a weaker structure as compared with the greater part of the paste being more fragile to mechanical loads [65]. In addition, a reduced level of chemical reactions is demonstrated in the presence of oil along with the weakening of cohesive forces [31].

Table 9. Mechanical compression properties of concrete in its different dosages

Material	F´c 28 days (MPa)						F´c 7 days (MPa)	F´c 28 days (MPa)
Age	7 days			14 days				
Sample	N° 1	N°2	N°3	N° 1	N°2	N°3		
C	26.5	25.79	25.72	33.042	32.23	32.08	26.0	32.5
CMF-02	19.8	20.01	18.93	28.243	27.91	27.74	19.6	28.0
CMF-04	18.351	195.4	17.78	29.342	28.76	28.44	18.4	28.9
CPF-02	19.078	193.3	18.42	26.114	25.65	25.66	18.8	25.8
CPF-04	25.525	252.7	24.57	28.754	28.56	29.04	25.0	28.8

This decrease in the F´c is similar to the ones reported by different authors adding up a small percentage of UEO in the concrete paste [66-70]. The percentage decrease of F'c with oil impregnation in the natural fibers ranges from 11.1% to 20% with respect to sample C, as can be seen in Figure 12. At the early curing time of 7 days, it can be observed that samples CMF-04 and CPF-02 have a lower development in their mechanical properties as a consequence of the hydrophobic characteristic of the UEO. This causes a delayed reaction of $Ca(OH)_2$, which has not yet been completely consumed for the production of calcium silicate hydrate (CSH); therefore, the bonding between the fiber and the matrix is poor [71].

Figure 12. Variations of compressive strength during the curing process

4.3. Flexural Behavior of Concrete Specimens

Average concrete flexural resistance (F´f) at 28 curing days is shown in Figure 13. The effects of the UEO on the flexural strength are negative, decreasing by 25% with respect to the control sample, and the incorporation of the fiber in the concrete paste does not prevent the propagation of cracks when the material is subjected to stresses. The Flexural strength of concrete decreases due to the weakened bond interface, the failure mode of the fibers is predominantly because of heavy metals present in the used oil engine, namely ZnO and P_2O_5 [20, 58]. With the use of UEO and fibers, a decrease in the mechanical properties of concrete has been reported elsewhere [72-74].
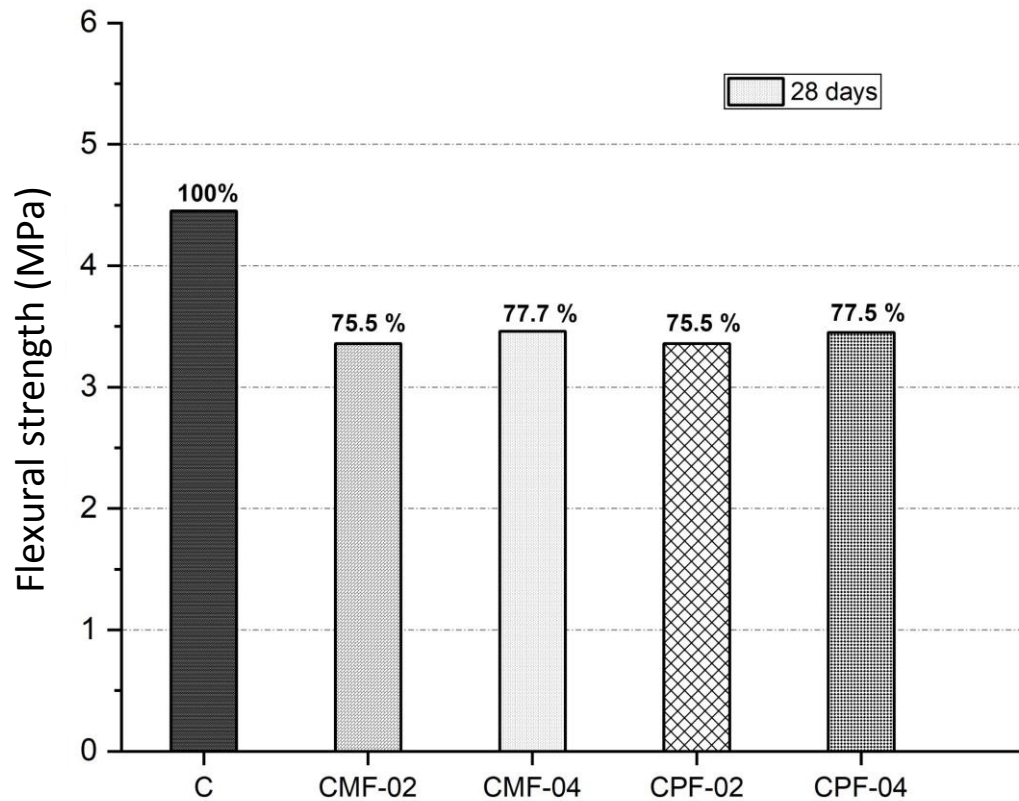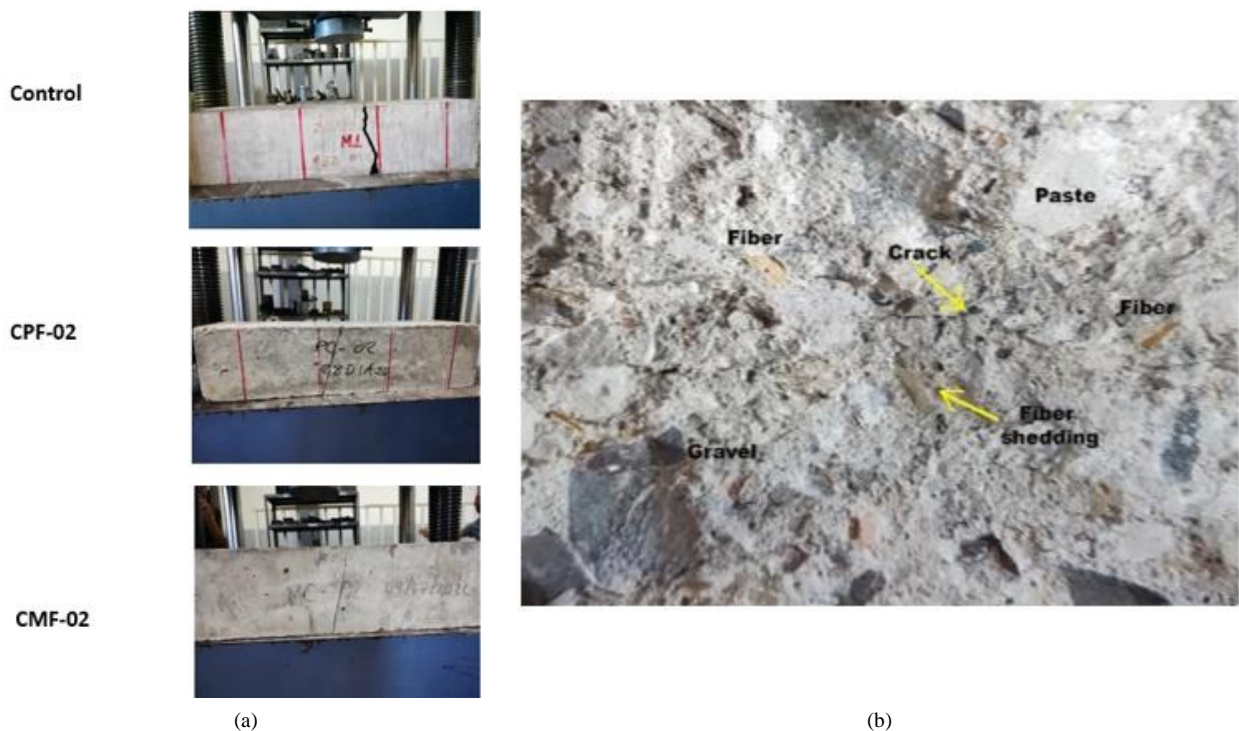
Figure 13. Variation of flexural strength of concrete with TNF, cured at 28 days

The results of the cracks in the flexural test are shown in Figure 14-a), as it can be generally noted that all specimens show a single crack passing through the center in the third of the beam. Specimen control shows a vertical crack characteristic of reinforced concrete; likewise, the specimens with natural fibers CPF-02 and CMF-02, show a brittle shear failure of diagonal type, as previously described the tensile strengths are low, the main cause is the null adhesion of the UEO treated fiber with the cement matrix as can be observed in Figure 14-b).

Figure 14. a) Fracture of specimens in flexural tests; b) Macro structure

4.4. Interpretation of Corrosion Potential E$_{corr}$

During the corrosion process, an electric current flow between the cathodic and anodic sites through the concrete and this flow can be detected by measuring the potential drop across the concrete [75]. Therefore, E$_{corr}$ corrosion potential measurement is a non-destructive method that detects these changes on the metal surface.

The corrosion potentials for the concrete samples with oil-treated fibers are shown in Figure 15. At the beginning of the monitoring, it is observed that the sample CMF-04, presents more positive E$_{corr}$ values of -100 mV compared to the other samples, placing it in a zone of 10% probability of corrosion. This phenomenon indicates a good distribution of the fibers that delay the transport of fluids and chloride ions [34].
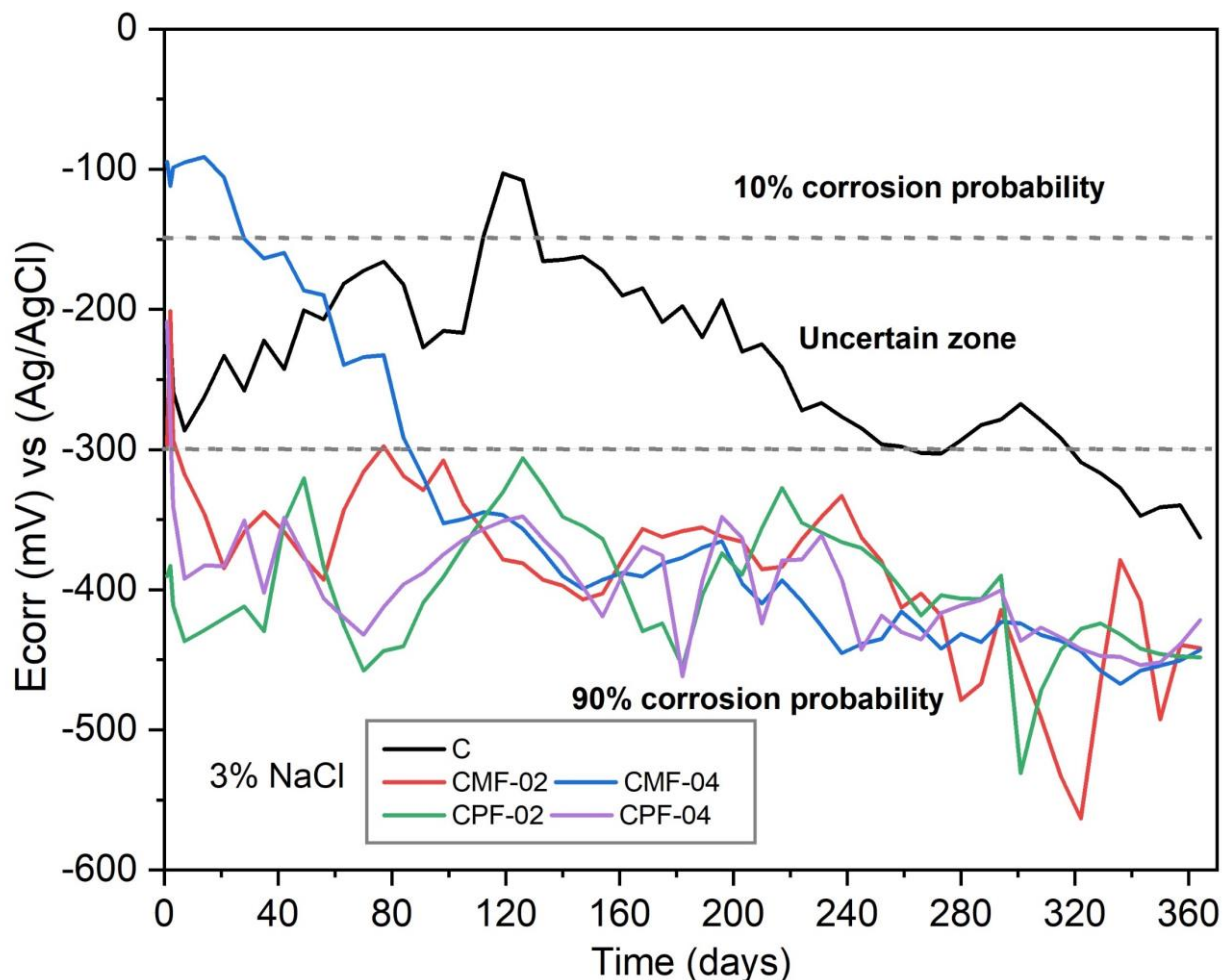

Figure 15. Corrosion potential values for structural steel

After 80 days the sample has a drop in E$_{corr}$ potentials entering a zone of uncertainty, as time progresses and on day 365 of exposure this sample acquires more negative values from -400 mV to -550 mV entering a zone of 90% probability of corrosion, this fact could mean the increase of chloride ion content solution on the surface of the steel/concrete interface [76]. Samples CMF-02, CPF-02 and CPF-04 are in an active zone with 90% probability of corrosion from the beginning to the end of the measurement days, due to the high porosity of the samples, which causes higher voids in the cement paste and higher concentrations of oxygen, water and chloride ions [77, 78]. Chloride and oxygen ions compete to reach the surface of the reinforcing steel through a diffusion phenomenon [79]

4.5. Interpretation of Electrochemical Noise Technique

The maintenance and repair of structural steel reinforced concrete for its safety needs effective monitoring and Inspection methods to evaluate the corrosion of steel reinforcement [80]. The aqueous chloride solution can quickly reach the embedded steel, so the onset of corrosion occurs in the metal [81]. Figures 16 and 17 show the results of Rn and the corrosion rate of concrete with treated fibers.
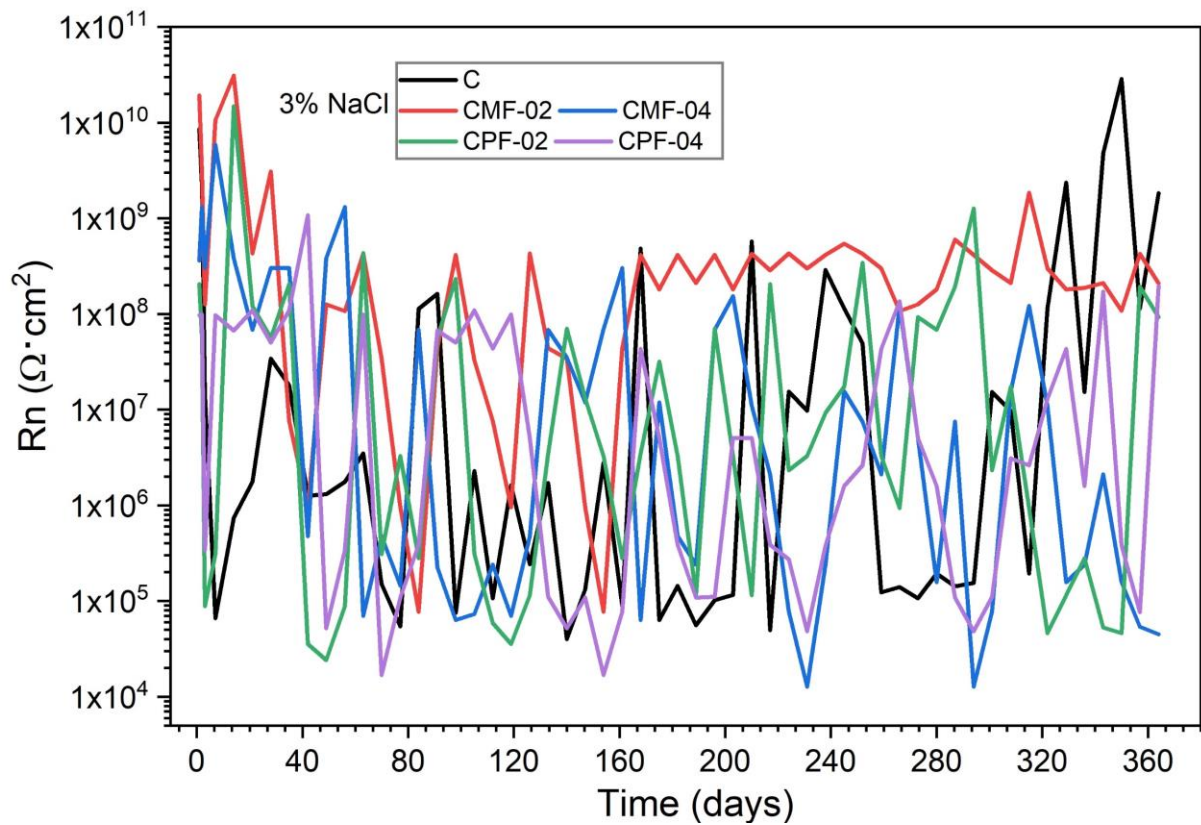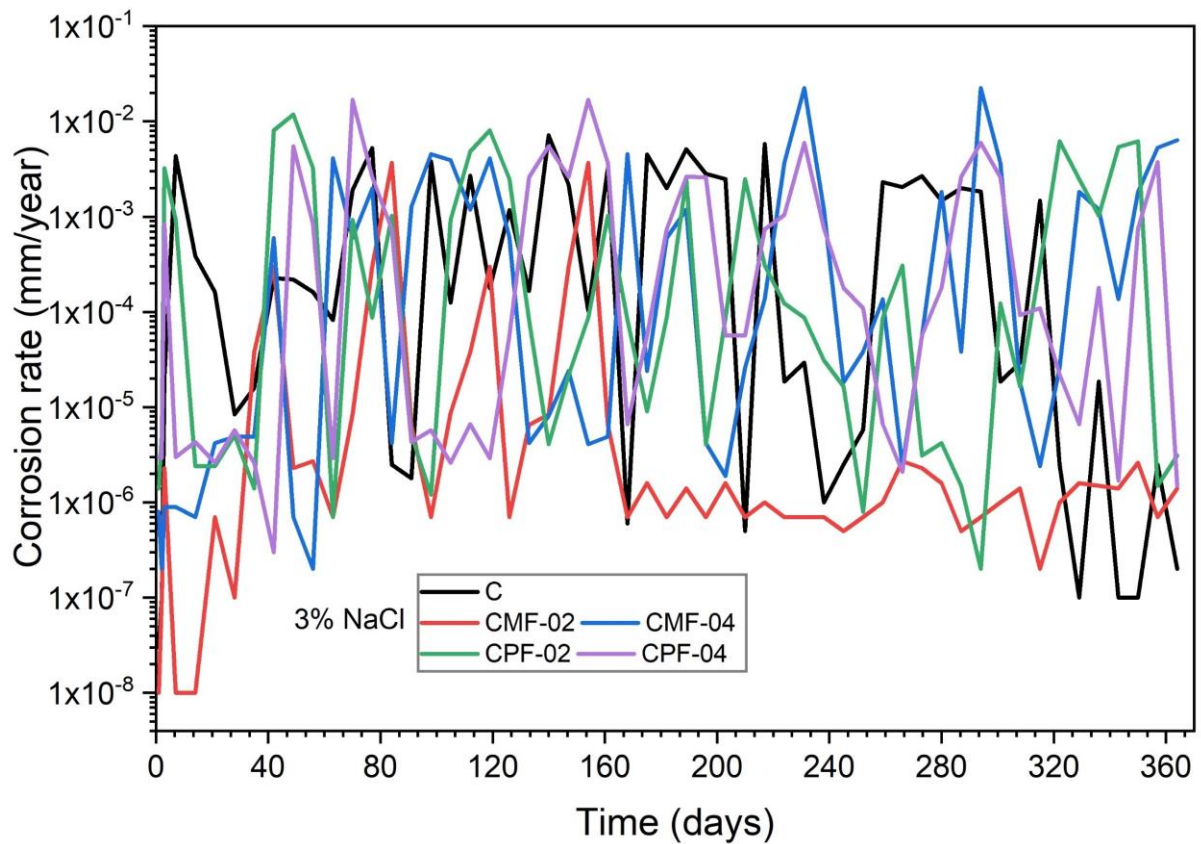
Figure 16. Rn values in the reinforced concrete

Figure 17. Corrosion rate for steel rod

On day 40 of monitoring, high and low transients of Rn with values between 1×10^{10} $\Omega \cdot cm^2$ and 1×10^5 $\Omega \cdot cm^2$ are observed for all samples, low values of Rn could indicate that the concentration of chloride ion increases on the surface of the steel bar, consequently, the corrosion rate is severe [82], i.e., the corrosion rate is inversely proportional to the values of Rn.

The values of UEO-treated samples are higher than the control sample, as the exposure time progresses the Rn values for natural fibers maintain the increase, high values of noise resistance, corrosion rate decreases, the entry of Cl- in the concrete increases the rate by the reduction of the alkaline hydrated products of the cement that passivates the embedded steel [83], i.e., the steel bars are passivated and depassivated by the interaction of the aggressive agents that were transported through the pore network of the concrete.

At the end of exposure, all samples show high and low Rn values, these fluctuations possibly due to passivation depassivation events transient behavior. It is not clear if the trend would continue as low or if it would follow the same trend as the control. However, sample CMF-02 shows high and constant Rn values of 1×10^9 Ω.cm^2 from day 160 to 365 days of exposure to the saline medium, this phenomenon may indicate that the treated fiber and the oil behave as a physical barrier, which may cause a slower diffusion of aggressive agents, also high Rn values indicate passivation in the metal and a negligible corrosion rate [46].

Quantitative information on the corrosion rate of steel is of utmost importance for the evaluation of repair methods, for service life prediction and for the structural evaluation of corroded elements [84].

An electrochemical parameter that can be obtained with the EN test is the type of corrosion that is present in the steel bars through the localization index results as shown in Figure 18. It has been argued in the literature that L.I., can be used to determine the nature of the type of corrosion with values approaching 1 being characteristic of localized corrosion [85].
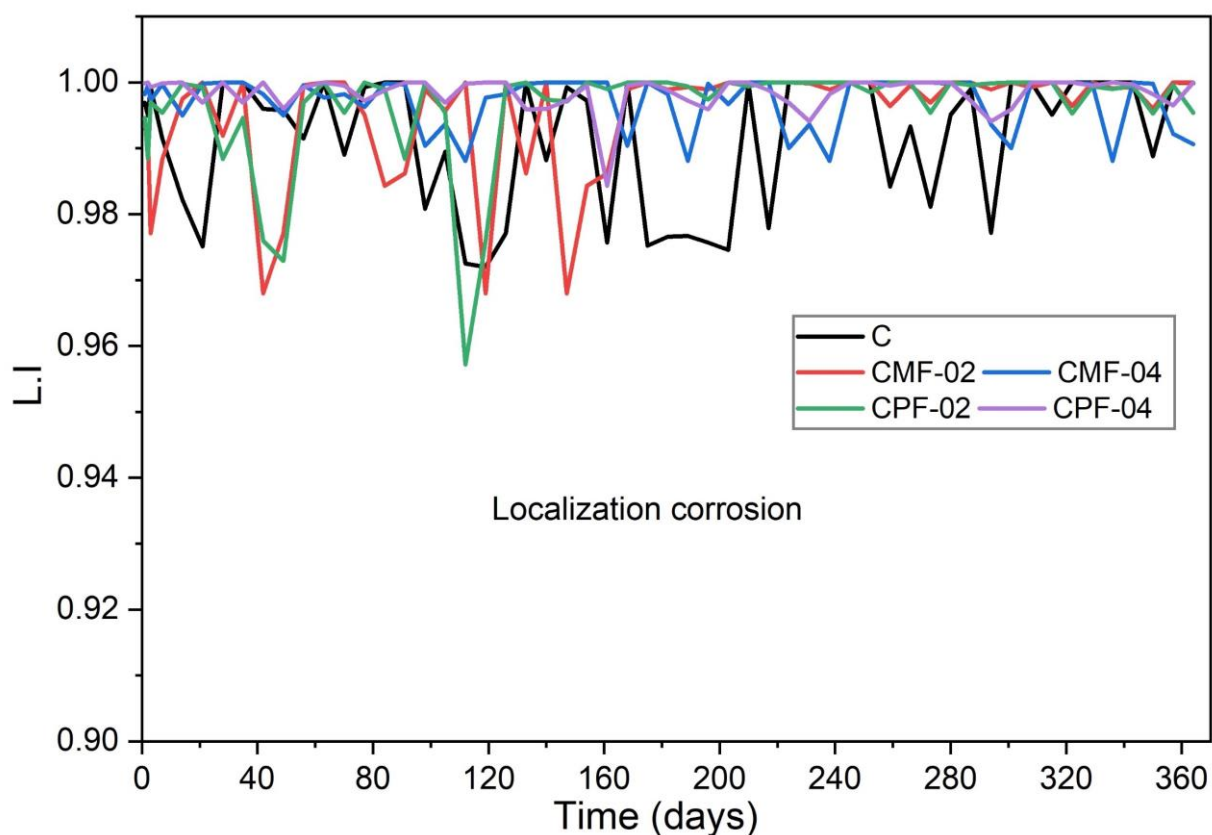

Figure 18. Type of corrosion in the steel/concrete system

It can be observed in a general way that all the samples with treated fibers have localized corrosion, that is, there are small areas of the rod surface, producing an important local reduction of the reinforcement section [64]. This type of corrosion is more likely to occur in reinforced concrete structures exposed to saline environments [86].

4.6. Interpretation of Linear Polarization Resistance

The values of the treated fiber concrete samples can be observed in Figure 19. At the beginning, all samples acquired Rp values of around 1×10^5 $\Omega \cdot$cm^2, indicating that the steel is under low corrosion attack. As the immersion time progresses on days 210 and 365 of monitoring, sample CMF-02 presents a rise in Rp behaviors as observed with high values of between 1×10^5 $\Omega \cdot$cm^2 and 1×10^7 $\Omega \cdot$cm^2, indicating a passivation in the metal surface and obtaining negligible corrosion damage as seen in Figure 20. Generally, steel corrosion is considered to be in the passive state if the current density is less than 0.1 mA/cm^2 and in the active state for values greater than 1 mA/cm^2 [44, 49]. The UEO has a positive effect on the corrosion rate by acting as a film or barrier around the metal; these results are comparable to those of other authors [87].
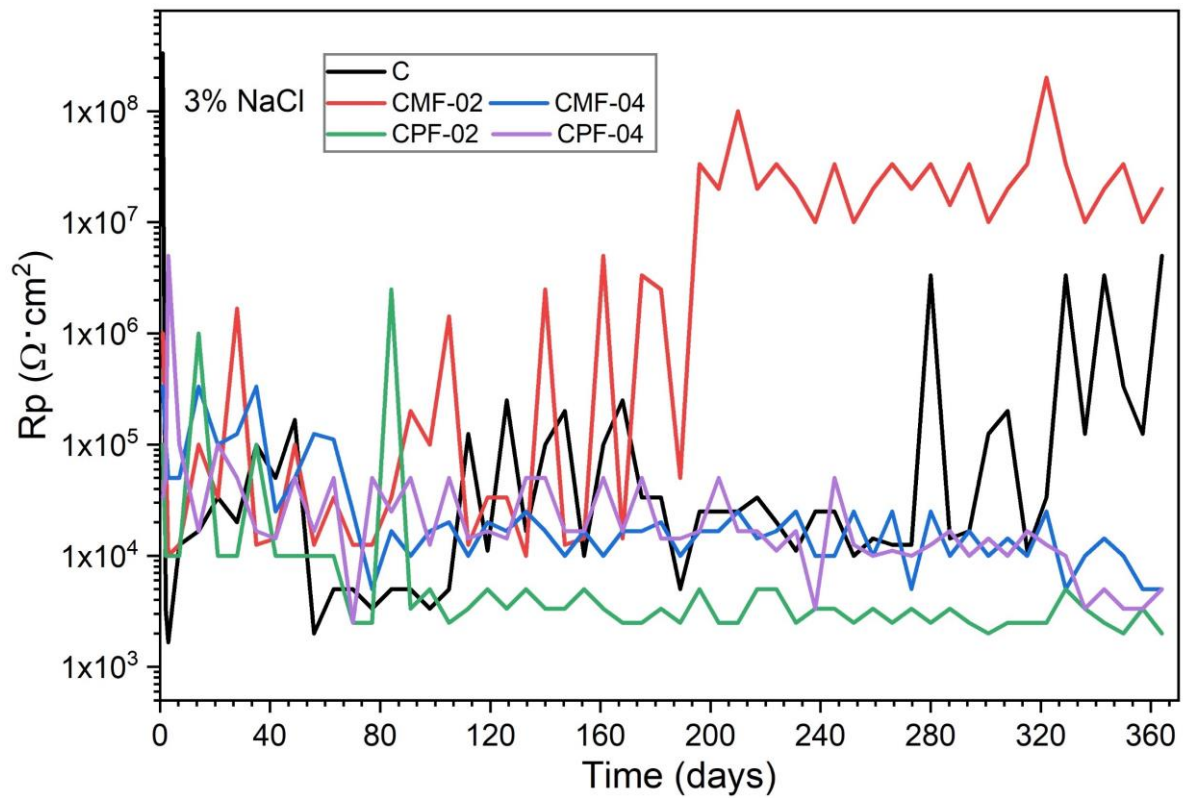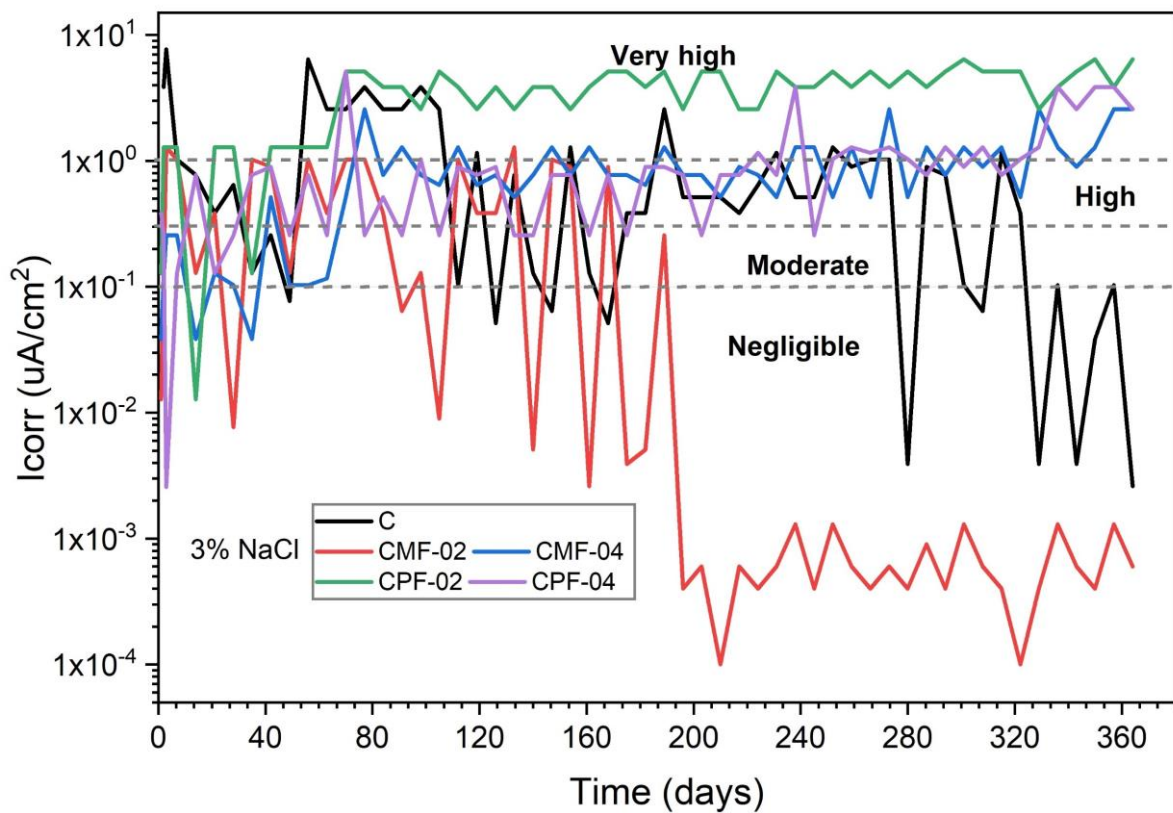
Figure 19. Average values of Rp

Figure 20. Current density values on the risk of steel corrosion

In the CPF-02 sample, low Rp values can be observed as the days of exposure progress, with values between 1×10^3 $\Omega.cm^2$ and 1×10^4 $\Omega.cm^2$ indicating high corrosion rate in the metal, due to poor adhesion of the fibers with the paste; likewise, the high porosity of the concrete paste by consequence has greater presence of oxygen diffusion and chloride

ions at the steel/paste interface, [88]. The values for the treated fibers have diverse from negligible to very high service life values compared to sample C. The samples CMF-04, CPF-02, and CPF-04 present very high Icorr values, increases in Icorr over time may not necessarily represent an increase in corrosion rate throughout the rebar, but rather the depassivation and initiation of active corrosion of greater amounts of rebar surface area [89]. Chloride penetration occurs mainly through capillary pores as free Cl- chlorides by adsorption, diffusion, and capillary permeation [90]. The amount of fibers has a direct influence on the degree of corrosion of reinforcing bars in concrete [77].

4.7. Electrochemical Impedance Interpretations

The graph of real Z' on the abscissa and imaginary Z" on the ordinate were measured from high to low frequencies which are called Nyquist diagrams [80], these graphs present loops related to time constants originating from the structure and reactions at the electrode [91]. For the interpretation of the diagrams, the loops generated in the test are analyzed. Generally, for reinforced concrete corrosion, graphs present two or three loops (capacitive arcs with or without inductive loop), whose centers are below the real axis (Zreal) and which are more or less separated [80, 91]. The high-frequency EIS spectra in the Nyquist diagram are usually a capacitive loop, which is generally attributed to the bulk concrete resistance representing Re the ohmic resistance of the solution in the pores based on the electrode reaction time, and at middle to low frequencies it is possible to attribute the low-frequency loop to a charge transfer process in combination with a mass transport process (Rp), while the straight line indicates a mechanism of ion diffusion through the pores [91-95].

The EIS results are shown in Figure 21, at the beginning of measurement at 24 hours, it can be widely observed that the control sample presents a better solution resistance Re and a higher impedance Rp, with values of $1x10^6$ and $1x10^7$ $\Omega \cdot cm^2$ this phenomenon can be explained by the low porosity.
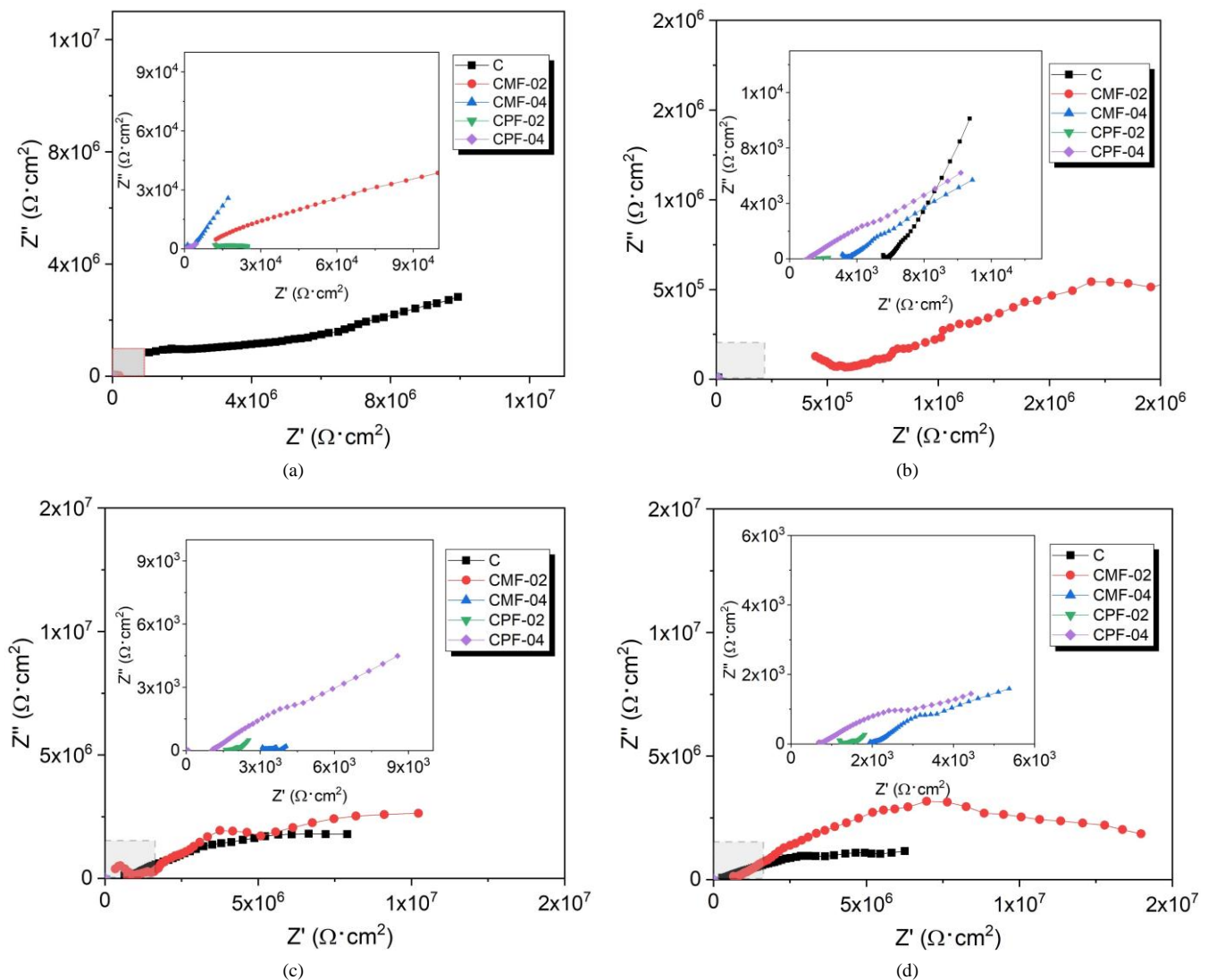

Figure 21. Nyquist diagrams for the days of a) 1, b) 168, c) 280, and d) 365

Small and depressed semicircles can be noticed for samples with treated fibers, indicating low Re and impedance values due to the presence of larger pores in the concrete, causing not only increased diffusion of chloride Cl- ions but also diffusion of O_2 and H_2O [54].

For day 168, a remarkable improvement can be noticed for the fibers treated with used oil; the sample CMF-02 presents a better Re as well as high impedance values of $1\times10^6\ \Omega\cdot cm^2$ with respect to the control sample. This fact could indicate the formation of a protective film of UEO on the metal surface by the high impedance values indicate a lower corrosion rate in the steel bar [96]. In addition, it was demonstrated that the physical properties of concrete, such as air content and porosity, have a direct relationship with corrosion damage to the metal due to the transport of species at the steel-concrete interface.

During the 240-day measurement, it was observed that the control sample had high values of Re and Rp of 1×10^7 $\Omega\cdot cm^2$, which could indicate passivation in the metal. At the end of the 365 days of monitoring, it is appreciated that the sample CMF-02 has had a positive response to the corrosion process of the steel for 168 days, maintaining a constant impedance until the end of the exposure. High values in this low-frequency region may be associated with the presence of the passive film [97, 98].

5. Conclusions

The following conclusions can be drawn:

- High levels of workability were obtained in all samples incorporating treated fibers from impregnated UEO acting as water reduction and lubricant in cement particles, and aggregates.

- The CPF-02 and CPF-04 samples present 133% and 123% air content greater values, when compared with the control sample, ascribed to UEO high absorption in palm fibers, weakening the adhesion in fibers and cement matrix. As a consequence, the increase in voids in the cement paste porosity increased by 34% and 33%, respectively.

- The UEO impregnated effect in fibers modified the low-level properties of mechanical compression in concrete. The CMF-04 specimen exhibited higher resistance when compared with the other treated samples but was lower than the control sample.

- The f´f of all samples treated showed a decrease between 22% and 25% compared to the sample without added fibers. The UEO modified the fiber surface, losing the rough texture and promoting concrete specimens to present a fragile cracking failure.

- The low performance in mechanical properties may be due to poor adherence and cohesion in fiber paste materials to support external forces and stresses.

- All samples presented a 90% probability of corrosion, with more negative values of corrosion potential ranging from -400 mV to -550 mV.

- The sample CMF-02 presented a better positive performance in the corrosion rate on the steel with high values of Rn and Rp of $1\times10^8\ \Omega\cdot cm^2$, indicating the formation of a protective film of UEO on the steel surface, decreasing the diffusion of Cl-, H20, and oxygen, and appreciating negligible corrosion damage on the road.

- In all samples, diffusion processes were observed on the steel/concrete interface, according to the EIS data.

6. Declarations

6.1. Author Contributions

6.2. Data Availability Statement

The data presented in this study are available on request from the corresponding author.

6.3. Funding

6.4. Acknowledgements

6.5. Conflicts of Interest

The authors declare no conflict of interest.

7. References

[1] Feng, W., Tarakbay, A., Ali Memon, S., Tang, W., & Cui, H. (2021). Methods of accelerating chloride-induced corrosion in steel-reinforced concrete: A comparative review. Construction and Building Materials, 289, 123165. doi:10.1016/j.conbuildmat.2021.123165.

[2] Van Steen, C., Nasser, H., Verstrynge, E., & Wevers, M. (2022). Acoustic emission source characterisation of chloride-induced corrosion damage in reinforced concrete. Structural Health Monitoring, 21(3), 1266–1286. doi:10.1177/14759217211013324.

[3] Tesic, K., Baricevic, A., Serdar, M., & Gucunski, N. (2023). Quantifying the impact of parameters of chloride-induced reinforcement corrosion on the GPR signal. Construction and Building Materials, 399, 132594. doi:10.1016/j.conbuildmat.2023.132594.

[4] Flores Nicolás, A., Menchaca Campos, E. C., Flores Nicolás, M., Martínez González, J. J., González Noriega, O. A., & Uruchurtu Chavarín, J. (2024). Influence of Recycled High-Density Polyethylene Fibers on the Mechanical and Electrochemical Properties of Reinforced Concrete. Fibers, 12(3), 24. doi:10.3390/fib12030024.

[5] Mohammed, M., Rahman, R., Mohammed, A. M., Adam, T., Betar, B. O., Osman, A. F., & Dahham, O. S. (2022). Surface treatment to improve water repellence and compatibility of natural fiber with polymer matrix: Recent advancement. Polymer Testing, 115. doi:10.1016/j.polymertesting.2022.107707.

[6] Juárez Alvarado, C. A., Rodríguez López, P., Rivera Villarreal, R., & Rechy de Von Roth, M. D. L. Á. (2004). Use of natural lechuguilla fibers as reinforcement in concrete. Ingenierías, 7(22), 7-19. (In Spanish).

[7] Juradin, S., Boko, I., Netinger Grubeša, I., Jozić, D., & Mrakovčić, S. (2021). Influence of different treatment and amount of Spanish broom and hemp fibres on the mechanical properties of reinforced cement mortars. Construction and Building Materials, 273, 121702. doi:10.1016/j.conbuildmat.2020.121702.

[8] Ferreira, S. R., Silva, F. de A., Lima, P. R. L., & Toledo Filho, R. D. (2017). Effect of hornification on the structure, tensile behavior and fiber matrix bond of sisal, jute and curauá fiber cement based composite systems. Construction and Building Materials, 139, 551–561. doi:10.1016/j.conbuildmat.2016.10.004.

[9] Xie, X., Zhou, Z., & Yan, Y. (2019). Flexural properties and impact behaviour analysis of bamboo cellulosic fibers filled cement-based composites. Construction and Building Materials, 220, 403–414. doi:10.1016/j.conbuildmat.2019.06.029.

[10] Lumingkewas, R. H., Husen, A., & Andrianus, R. (2017). Effect of Fibers Length and Fibers Content on the Splitting Tensile Strength of Coconut Fibers Reinforced Concrete Composites. Key Engineering Materials, 748, 311–315. doi:10.4028/www.scientific.net/kem.748.311.

[11] Machaka, M., Basha, H., Abou Chakra, H., & Elkordi, A. (2014). Alkali treatment of fan palm natural fibers for use in fiber reinforced concrete. European Scientific Journal, 10(12), 186-195.

[12] Madhwani, H., Sathyan, D., & Mini, K. M. (2019). Study on durability and hardened state properties of sugarcane bagasse fiber reinforced foam concrete. Materials Today: Proceedings, 46, 4782–4787. doi:10.1016/j.matpr.2020.10.313.

[13] Ighalo, J. O., Adeyanju, C. A., Ogunniyi, S., Adeniyi, A. G., & Abdulkareem, S. A. (2021). An empirical review of the recent advances in treatment of natural fibers for reinforced plastic composites. Composite Interfaces, 28(9), 925–960. doi:10.1080/09276440.2020.1826274.

[14] Ahmad, J., & Zhou, Z. (2022). Mechanical Properties of Natural as well as Synthetic Fiber Reinforced Concrete: A Review. Construction and Building Materials, 333, 127353. doi:10.1016/j.conbuildmat.2022.127353.

[15] Ramamoorthy, S. K., Di, Q., Adekunle, K., & Skrifvars, M. (2012). Effect of water absorption on mechanical properties of soybean oil thermosets reinforced with natural fibers. Journal of Reinforced Plastics and Composites, 31(18), 1191–1200. doi:10.1177/0731684412455257.

[16] Kim, H., & Seo, D. (2007). Influence of water saturation on fracture toughness in woven natural fiber reinforced composites. Advanced Composite Materials, 16(2), 83–94. doi:10.1163/156855107780918955.

[17] Symington, M. C., Banks, W. M., West, O. D., & Pethrick, R. A. (2009). Tensile testing of cellulose based natural fibers for structural composite applications. Journal of Composite Materials, 43(9), 1083–1108. doi:10.1177/0021998308097740.

[18] Zhang, D., Tan, K. H., Dasari, A., & Weng, Y. (2020). Effect of natural fibers on thermal spalling resistance of ultra-high-performance concrete. Cement and Concrete Composites, 109, 103512. doi:10.1016/j.cemconcomp.2020.103512.

[19] Shah, I., Li, J., Yang, S., Zhang, Y., & Anwar, A. (2022). Experimental Investigation on the Mechanical Properties of Natural Fiber Reinforced Concrete. Journal of Renewable Materials, 10(5), 1307–1320. doi:10.32604/jrm.2022.017513.

[20] Onuaguluchi, O., & Banthia, N. (2016). Plant-based natural fibre reinforced cement composites: A review. Cement and Concrete Composites, 68, 96–108. doi:10.1016/j.cemconcomp.2016.02.014.

[21] Paricaguán, B., Albano, C., Palacios, J., Torres, R., Camacho, N., Infante, J., & Alvarado, M. (2013). Thermal degradation of coconut fibers with chemical treatment from concrete mixtures (Kinetic Study). Revista Ingeniería UC, 20(2), 60-67.

[22] Li, M., Pu, Y., Thomas, V. M., Yoo, C. G., Ozcan, S., Deng, Y., Nelson, K., & Ragauskas, A. J. (2020). Recent advancements of plant-based natural fiber–reinforced composites and their applications. Composites Part B: Engineering, 200, 108254. doi:10.1016/j.compositesb.2020.108254.

[23] Zhang, K., Cao, Q., Jin, L., Li, P., & Zhang, X. (2017). A novel route to utilize waste engine oil by blending it with water and coal. Journal of Hazardous Materials, 332, 51–58. doi:10.1016/j.jhazmat.2017.02.052.

[24] Chen, H., Qin, R., & Lau, D. (2021). Recycling used engine oil in concrete design mix: An ecofriendly and feasible solution. Journal of Cleaner Production, 329, 129555. doi:10.1016/j.jclepro.2021.129555.

[25] Yousif, B. F., Orupabo, C., & Azwa, Z. N. (2013). Characteristics of Kenaf Fiber Immersed in Different Solutions. Journal of Natural Fibers, 9(4), 207–218. doi:10.1080/15440478.2012.733149.

[26] Wong, C., McGowan, T., Bajwa, S. G., & Bajwa, D. S. (2016). Impact of fiber treatment on the oil absorption characteristics of plant fibers. BioResources, 11(3), 6452–6463. doi:10.15376/biores.11.3.6452-6463.

[27] Ramli, M., Kwan, W. H., & Abas, N. F. (2013). Strength and durability of coconut-fiber-reinforced concrete in aggressive environments. Construction and Building Materials, 38, 554–566. doi:10.1016/j.conbuildmat.2012.09.002.

[28] ASTM C150/C150. (2021). Standard Specification for Portland Cement. ASTM International, Pennsylvania, United States. doi:10.1520/C0150_C0150M-20.

[29] Martinez, S., Teresa, M., Sánchez Herrera, L. M., Torres García, G., & Garcia Paredes, J. D. (2012). Value network of mango and its waste based on nutritional and functional properties. Revista Mexicana de Agronegocios, 1-30.

[30] Escalante, M. A. M. (2018). Cultural appropriation: The case of traditional crafts. Anales del Museo Nacional de Antropología. Dirección General de Bellas Artes y de Conservación y Restauración de Bienes Culturales. Available online: https://dialnet.unirioja.es/servlet/revista?codigo=81 (accessed on March 2024).

[31] Djafari Petroudy, S. R. (2017). Physical and mechanical properties of natural fibers. In Advanced High Strength Natural Fibre Composites in Construction: Woodhead Publishing, 59–83. doi:10.1016/B978-0-08-100411-1.00003-0.

[32] Mújica-Paz, H., Valdez-Fragoso, A., López-Malo, A., Palou, E., & Welti-Chanes, J. (2003). Impregnation properties of some fruits at vacuum pressure. Journal of Food Engineering, 56(4), 307–314. doi:10.1016/S0260-8774(02)00155-3.

[33] Ferreira, D. P., Cruz, J., & Fangueiro, R. (2018). Surface modification of natural fibers in polymer composites. In Green Composites for Automotive Applications: Woodhead Publishing 3–41. doi:10.1016/B978-0-08-102177-4.00001-X.

[34] Assaad, J. J. (2013). Disposing used engine oils in concrete - Optimum dosage and compatibility with water reducers. Construction and Building Materials, 44, 734–742. doi:10.1016/j.conbuildmat.2013.03.078.

[35] Shafiq, N., Choo, C. S., & Isa, M. H. (2018). Effects of used engine oil on slump, compressive strength and oxygen permeability of normal and blended cement concrete. Construction and Building Materials, 187, 178–184. doi:10.1016/j.conbuildmat.2018.07.195.

[36] Sekar, S., Suresh Kumar, S., Vigneshwaran, S., & Velmurugan, G. (2020). Evaluation of Mechanical and Water Absorption Behavior of Natural Fiber-Reinforced Hybrid Biocomposites. Journal of Natural Fibers, 19(5), 1–11. doi:10.1080/15440478.2020.1788487.

[37] Sumesh, K. R., Kavimani, V., Rajeshkumar, G., Indran, S., & Khan, A. (2022). Mechanical, water absorption and wear characteristics of novel polymeric composites: Impact of hybrid natural fibers and oil cake filler addition. Journal of Industrial Textiles, 51(4), 5910S-5937S. doi:10.1177/1528083720971344.

[38] Nine, M. J., Kabiri, S., Sumona, A. K., Tung, T. T., Moussa, M. M., & Losic, D. (2020). Superhydrophobic/superoleophilic natural fibres for continuous oil-water separation and interfacial dye-adsorption. Separation and Purification Technology, 233, 116062. doi:10.1016/j.seppur.2019.116062.

[39] ASTM C143/C143M-20. (2020). Standard Test Method for Slump of Hydraulic-Cement Concrete. ASTM International, Pennsylvania, United States. doi:10.1520/C0143_C0143M-20.

[40] ASTM C231/C231M-22. (2024). Standard Test Method for Air Content of Freshly Mixed Concrete by the Pressure Method. ASTM International, Pennsylvania, United States. doi:10.1520/C0231_C0231M-22.

[41] ASTM C31/C31M-23. (2024). Standard Practice for Making and Curing Concrete Test Specimens in the Field. ASTM International, Pennsylvania, United States. doi:10.1520/C0031_C0031M-23.

[42] ASTM C78/C78M-22. (2022). Standard Test Method for Flexural Strength of Concrete (Using Simple Beam with Center-Point Loading). ASTM International, Pennsylvania, United States. doi:10.1520/C0078_C0078M-22.

[43] Yaowarat, T., Suddeepong, A., Hoy, M., Horpibulsuk, S., Takaikaew, T., Vichitcholchai, N., Arulrajah, A., & Chinkulkijniwat, A. (2021). Improvement of flexural strength of concrete pavements using natural rubber latex. Construction and Building Materials, 282, 122704. doi:10.1016/j.conbuildmat.2021.122704.

[44] Rodrigues, R., Gaboreau, S., Gance, J., Ignatiadis, I., & Betelu, S. (2021). Reinforced concrete structures: A review of corrosion mechanisms and advances in electrical methods for corrosion monitoring. Construction and Building Materials, 269, 121240. doi:10.1016/j.conbuildmat.2020.121240.

[45] ASTM C876-09. (2016). Standard Test Method for Corrosion Potentials of Uncoated Reinforcing Steel in Concrete. ASTM International, Pennsylvania, United States. doi:10.1520/C0876-09.

[46] Flores-Nicolás, A., Flores-Nicolás, M., & Uruchurtu-Chavarín, J. (2021). Corrosion effect on reinforced concrete with the addition of graphite powder and its evaluation on physical-electrochemical properties. Revista ALCONPAT, 11(1), 18–33. doi:10.21041/ra.v11i1.501.

[47] Mills, D., Lambert, P., & Yang, S. (2021). Electrochemical noise measurement to assess corrosion of steel reinforcement in concrete. Materials, 14(18), 5392. doi:10.3390/ma14185392.

[48] Calabrese, L., Galeano, M., & Proverbio, E. (2023). Data Mining Applied to the Electrochemical Noise Technique in the Time/Frequency Domain for Stress Corrosion Cracking Recognition. Corrosion and Materials Degradation, 4(4), 659–679. doi:10.3390/cmd4040034.

[49] Andrade, C., & Alonso, C. (2004). Test methods for on-site corrosion rate measurement of steel reinforcement in concrete by means of the polarization resistance method. Materials and Structures, 37(9), 623–643. doi:10.1007/bf02483292.

[50] ASTM G59-97. (2020). Standard Test Method for Conducting Potentiodynamic Polarization Resistance Measurements. ASTM International, Pennsylvania, United States. doi:10.1520/G0059-97R20.

[51] Lukács, Z., & Kristóf, T. (2023). Linear transformations of the Butler–Volmer equation. Electrochemistry Communications, 154, 107556. doi:10.1016/j.elecom.2023.107556.

[52] Román, A. S., Barrientos, M. S., Harms, F., Mendez, C. M., & Ares, A. E. (2016, March). Corrosion resistance of AISI 304L stainless steel in soy biodiesel. Anales (Asociación Física Argentina), 27(1). (In Spanish).

[53] Sohail, M. G., Laurens, S., Deby, F., Balayssac, J. P., & Al Nuaimi, N. (2021). Electrochemical corrosion parameters for active and passive reinforcing steel in carbonated and sound concrete. Materials and Corrosion, 72(12), 1854–1871. doi:10.1002/maco.202112569.

[54] Da, B., Yu, H., Ma, H., & Wu, Z. (2018). Reinforcement corrosion research based on the linear polarization resistance method for coral aggregate seawater concrete in a marine environment. Anti-Corrosion Methods and Materials, 65(5), 458–470. doi:10.1108/acmm-03-2018-1911.

[55] Niu, S., Luo, J., Chen, M. T., Chen, Z., Wang, X., Bai, X., & Li, J. (2023). Experimental study of cement-based materials under sulfate attack environment using Electrochemical Impedance Spectroscopy. International Journal of Electrochemical Science, 18(5), 100133. doi:10.1016/j.ijoes.2023.100133.

[56] Sobhani, J., & Najimi, M. (2013). Electrochemical impedance behavior and transport properties of silica fume contained concrete. Construction and Building Materials, 47, 910–918. doi:10.1016/j.conbuildmat.2013.05.010.

[57] Björnström, J., & Chandra, S. (2003). Effect of superplasticizers on the rheological properties of cements. Materials and Structures, 36(10), 685–692. doi:10.1007/bf02479503.

[58] Varghese, R., & Eapen Sakaria, P. (2017). Experimental Investigation on the Properties of Fresh and Hardened Concrete with Used Engine Oil as Super Plasticizer. International Research Journal of Engineering and Technology, 04(05), 2230–2236. doi:10.13140/RG.2.2.26601.34400.

[59] Hasan, B., & Ali, M. (2023). Potential of used-petrol-engine-oil as an admixture in cement composites: A detailed review. AIP Conference Proceedings. doi:10.1063/5.0129983.

[60] Lian, C., Zhuge, Y., & Beecham, S. (2011). The relationship between porosity and strength for porous concrete. Construction and Building Materials, 25(11), 4294–4298. doi:10.1016/j.conbuildmat.2011.05.005.

[61] Solís-Carcaño, R. Ó. M. E. L., & Moreno, E. I. (2006). Analysis of the porosity of concrete with limestone aggregate. Revista de la Facultad de Ingeniería de la UCV, 21(3), 57-68. (In Spanish).

[62] Solís Carcaño, R. G., & Alcocer Fraga, M. Á. (2019). Durabilidad del concreto con agregados de alta absorción. Ingeniería Investigación y Tecnología, 20(4), 1–13. doi:10.22201/fi.25940732e.2019.20n4.039. (In Spanish).

[63] Wang, L., Jin, M., Guo, F., Wang, Y. A. N., & Tang, S. (2021). Pore structural and fractal analysis of the influence of fly ash and silica fume on the mechanical property and abrasion resistance of concrete. Fractals, 29(2), 2140003. doi:10.1142/S0218348X2140003X.

[64] Nicolás, A. F. (2021). Evaluation of the corrosion and protection of reinforcing steel embedded in concrete in the presence of graphite and its effect on the mechanical-electrochemical properties. Master Thesis, Universidad Autónoma del Estado de Morelos, Cuernavaca, Mexico. (In Spanish).

[65] Yaphary, Y. L., Lam, R. H. W., & Lau, D. (2020). Reduction in cement content of normal strength concrete with used engine oil (UEO) as chemical admixture. Construction and Building Materials, 261, 119967. doi:10.1016/j.conbuildmat.2020.119967.

[66] Shafiq, N., Nuruddin, M. F., & Beddu, S. (2011). Properties of concrete containing used engine oil. International Journal of Sustainable Construction Engineering and Technology, 2(1), 72-82.

[67] Abdelaziz, G. E. (2011). Utilization of used-engine oil in concrete as a chemical admixture. Benha University, Egypt, 14-17.

[68] Burbano-Garcia, C., Hurtado, A., Silva, Y. F., Delvasto, S., & Araya-Letelier, G. (2021). Utilization of waste engine oil for expanded clay aggregate production and assessment of its influence on lightweight concrete properties. Construction and Building Materials, 273, 121677. doi:10.1016/j.conbuildmat.2020.121677.

[69] Alsadey, S. (2018). Effects of used engine oil as chemical admixture in concrete. International Journal of Energy and Sustainable Development, 3(2), 38-43.

[70] Attom, M., Hawileh, R., & Naser, M. (2013). Investigation on concrete compressive strength mixed with sand contaminated by crude oil products. Construction and Building Materials, 47, 99–103. doi:10.1016/j.conbuildmat.2013.04.042.

[71] Zhou, X., Saini, H., & Kastiukas, G. (2017). Engineering properties of treated natural hemp fiber-reinforced concrete. Frontiers in Built Environment, 3, 33. doi:10.3389/fbuil.2017.00033.

[72] Hussen, S. S. (2016). Using of Industrial Waste as a Green Chemical Admixture in Concrete. Kufa Journal of Engineering, 7(1), 104–114. doi:10.30572/2018/kje/711216.

[73] Al-Attar, T. S. (2013). A quantitative evaluation of bond strength between coarse aggregate and cement mortar in concrete. European scientific journal, 9(6).

[74] Nadeem, H., Habib, N. Z., Aun, N. C., Zoorob, S. E., Mustaffa, Z., Mesney, R., & Suubitaa, S. (2017). Used engine oil as alternate binder for buildings - A comparative study. Proceedings of Institution of Civil Engineers: Waste and Resource Management, 170(2), 57–65. doi:10.1680/jwarm.17.00005.

[75] Song, H. W., & Saraswathy, V. (2007). Corrosion monitoring of reinforced concrete structures - A review. International Journal of Electrochemical Science, 2(1), 1–28. doi:10.1016/s1452-3981(23)17049-0.

[76] Yodsudjai, W., & Pattarakittam, T. (2017). Factors influencing half-cell potential measurement and its relationship with corrosion level. Measurement: Journal of the International Measurement Confederation, 104, 159–168. doi:10.1016/j.measurement.2017.03.027.

[77] Kakooei, S., Akil, H. M., Dolati, A., & Rouhi, J. (2012). The corrosion investigation of rebar embedded in the fibers reinforced concrete. Construction and Building Materials, 35, 564–570. doi:10.1016/j.conbuildmat.2012.04.051.

[78] Sappakittipakorn, M., & Banthia, N. (2012). Corrosion of rebar and role of fiber reinforced concrete. Journal of Testing and Evaluation, 40(1). doi:10.1520/jte103873.

[79] Andrade, C., & Alonso, C. (1996). Corrosion rate monitoring in the laboratory and on-site. Construction and Building Materials, 10(5), 315–328. doi:10.1016/0950-0618(95)00044-5.

[80] Daniyal, M., & Akhtar, S. (2020). Corrosion assessment and control techniques for reinforced concrete structures: a review. Journal of Building Pathology and Rehabilitation, 5(1), 1–20. doi:10.1007/s41024-019-0067-3.

[81] Paul, S., van Zijl, G., & Šavija, B. (2020). Effect of Fibers on Durability of Concrete: A Practical Review. Materials, 13(20), 4562. doi:10.3390/ma13204562.

[82] Zhao, B., Li, J. H., Hu, R. G., Du, R. G., & Lin, C. J. (2007). Study on the corrosion behavior of reinforcing steel in cement mortar by electrochemical noise measurements. Electrochimica Acta, 52(12), 3976–3984. doi:10.1016/j.electacta.2006.11.015.

[83] Almashakbeh, Y., Saleh, E., & Al-Akhras, N. M. (2022). Evaluation of Half-Cell Potential Measurements for Reinforced Concrete Corrosion. Coatings, 12(7), 975. doi:10.3390/coatings12070975.

[84] Alexandre Reginato, L., Somensi Lorenzi, L., & Carlos Pinto da Silva Filho, L. (2023). Corrosion in reinforced concrete: Diagnostics through Potential Corrosion Technique. doi:10.21203/rs.3.rs-3156721/v3.

[85] Mansfeld, F., Sun, Z., & Hsu, C. H. (2001). Electrochemical noise analysis (ENA) for active and passive systems in chloride media. Electrochimica Acta, 46(24–25), 3651–3664. doi:10.1016/s0013-4686(01)00643-0.

[86] Darmawan, M. S. (2010). Pitting corrosion model for reinforced concrete structures in a chloride environment. Magazine of Concrete Research, 62(2), 91–101. doi:10.1680/macr.2008.62.2.91.

[87] Dharma, S., Silitonga, A. S., Shamsuddin, A. H., Sebayang, A. H., Milano, J., Sebayang, R., Sarjianto, Ibrahim, H., Bahri, N., Ginting, B., & Damanik, N. (2023). Properties and corrosion behaviors of mild steel in biodiesel-diesel blends. Energy Sources, Part A: Recovery, Utilization and Environmental Effects, 45(2), 3887–3899. doi:10.1080/15567036.2019.1668883.

[88] Andrade, C. (2019). Propagation of reinforcement corrosion: principles, testing and modelling. Materials and Structures/Materiaux et Constructions, 52(1), 2. doi:10.1617/s11527-018-1301-1.

[89] Blunt, J., Jen, G., & Ostertag, C. P. (2015). Enhancing corrosion resistance of reinforced concrete structures with hybrid fiber reinforced concrete. Corrosion Science, 92, 182–191. doi:10.1016/j.corsci.2014.12.003.

[90] Bertolini, L., Elsener, B., Pedeferri, P., Redaelli, E., & Polder, R. B. (2013). Corrosion of steel in concrete: prevention, diagnosis, repair. John Wiley & Sons, Hoboken, United States.

[91] Hoshi, Y., Koike, T., Tokieda, H., Shitanda, I., Itagaki, M., & Kato, Y. (2019). Non-Contact Measurement to Detect Steel Rebar Corrosion in Reinforced Concrete by Electrochemical Impedance Spectroscopy. Journal of The Electrochemical Society, 166(11), C3316–C3319. doi:10.1149/2.0371911jes.

[92] Dhouibi, L., Triki, E., & Raharinaivo, A. (2002). The application of electrochemical impedance spectroscopy to determine the long-term effectiveness of corrosion inhibitors for steel in concrete. Cement and Concrete Composites, 24(1), 35–43. doi:10.1016/S0958-9465(01)00062-2.

[93] Ribeiro, D. V., & Abrantes, J. C. C. (2016). Application of electrochemical impedance spectroscopy (EIS) to monitor the corrosion of reinforced concrete: A new approach. Construction and Building Materials, 111, 98–104. doi:10.1016/j.conbuildmat.2016.02.047.

[94] Song, G. (2000). Equivalent circuit model for AC electrochemical impedance spectroscopy of concrete. Cement and Concrete Research, 30(11), 1723–1730. doi:10.1016/S0008-8846(00)00400-2.

[95] Park, J., & Jung, M. (2021). Evaluation of the corrosion behavior of reinforced concrete with an inhibitor by electrochemical impedance spectroscopy. Materials, 14(19), 5508. doi:10.3390/ma14195508.

[96] Dorothy, R., Sasilatha, T., & Rajendran, S. (2021). Corrosion resistance of mild steel (Hull plate) in sea water in the presence of a coating of an oil extract of plant materials. International Journal of Corrosion and Scale Inhibition, 10(2), 676–699. doi:10.17675/2305-6894-2021-10-2-13.

[97] Fattah-alhosseini, A., Taheri Shoja, S., Heydari Zebardast, B., & Mohamadian Samim, P. (2011). An Electrochemical Impedance Spectroscopic Study of the Passive State on AISI 304 Stainless Steel. International Journal of Electrochemistry, 2011, 1–8. doi:10.4061/2011/152143.

[98] Cellat, K., Tezcan, F., Beyhan, B., Kardaş, G., & Paksoy, H. (2017). A comparative study on corrosion behavior of rebar in concrete with fatty acid additive as phase change material. Construction and Building Materials, 143, 490–500. doi:10.1016/j.conbuildmat.2017.03.165.